Letter

Nonergodicity of reset geometric Brownian motion

Deepak Vinod [1,*] Andrey G. Cherstvy [2,1,†] Wei Wang [3,‡] Ralf Metzler [1,§] and Igor M. Sokolov [2,4,‖]

[1] *Institute of Physics and Astronomy, University of Potsdam, 14476 Potsdam-Golm, Germany*
[2] *Institut für Physik, Humboldt-Universität zu Berlin, 12489 Berlin, Germany*
[3] *Max Planck Institute for the Physics of Complex Systems, 01187 Dresden, Germany*
[4] *IRIS Adlershof, 12489 Berlin, Germany*

(Received 12 October 2021; accepted 10 January 2022; published 31 January 2022)

We derive. the ensemble- and time-averaged mean-squared displacements (MSD, TAMSD) for Poisson-reset geometric Brownian motion (GBM), in agreement with simulations. We find MSD and TAMSD saturation for frequent resetting, quantify the spread of TAMSDs via the ergodicity-breaking parameter and compute distributions of prices. General MSD-TAMSD nonequivalence proves reset GBM nonergodic.

DOI: 10.1103/PhysRevE.105.L012106

Introduction. Prices of lookback-, barrier-, reset-, and range-type options [1–10] innately depend on their "path", $S(t)$ [on crossing min and max prices, being in certain ranges at preset times, etc., with prices adjusted on specific dates regularly or upon exceeding thresholds]. "Corrections" of option-pricing models, often using geometric Brownian motion (GBM), are thus needed. We study here the mean-squared displacement (MSD), time-averaged MSD (TAMSD) [19–21], probability-density function (PDF), and ergodicity-breaking parameter (EB) of reset [11–18] GBM.

GBM: Theory. GBM $S(t)$ solves the multiplicative-noise stochastic differential equation (Itô interpretation),

$$dS(t) = \mu S(t)dt + \sigma S(t)dW(t), \tag{1}$$

where μ and σ are [constant] drift and volatility. The Wiener-process increment $dW(t)$ is white Gaussian zero-mean noise. Exp-growing GBM (using Itô's lemma), $S(t) = S_0e^{(\mu-\sigma^2/2)t+\sigma W(t)}$ has the log-normal PDF,

$$P_0(S,t) = \frac{\exp[-[\ln(S/S_0) - (\mu-\sigma^2/2)t]^2/(2\sigma^2 t)]}{\sqrt{2\pi\sigma^2 t S^2}}, \tag{2}$$

that [with the initial price $S_0 = S(0)$] gives [19–21] the first two moments $\langle S(t)\rangle = S_0e^{\mu t}$ and $\langle S^2(t)\rangle = S_0^2 e^{(2\mu+\sigma^2)t}$ [with $\mathrm{MSD}(t) = \langle (S(t)-S_0)^2\rangle$], whereas the variance is $\mathrm{Var}(t) = \langle (S(t) - \langle S(t)\rangle)^2\rangle = S_0^2 e^{2\mu t}(e^{\sigma^2 t} - 1)$.

For a time series $S_i(t)$ of length T the TAMSD is [22] $\overline{\delta_i^2(\Delta)} = \frac{1}{T-\Delta}\int_0^{T-\Delta}[S_i(t+\Delta) - S_i(t)]^2 dt$. The angular brackets (overline) denote averaging over noise (time). For an ergodic process [22] the mean TAMSD $\langle\overline{\delta^2(\Delta)}\rangle = \frac{1}{N}\sum_{i=1}^{N}\overline{\delta_i^2(\Delta)}$ equals the MSD at $\Delta/T \ll 1$. For GBM [19–21] with $\mu = 0$ (considered below),

$$\langle\overline{\delta^2(\Delta)}\rangle = \frac{S_0^2}{\sigma^2(T-\Delta)}\left(e^{\sigma^2\Delta} - 1\right)\left(e^{\sigma^2(T-\Delta)} - 1\right) \tag{3}$$

behaves at short lag times as $\langle\overline{\delta^2(\Delta)}\rangle \approx \langle S^2(T)\rangle\Delta/T$.

Reset GBM: Theory. The Poissonian waiting-time distribution $\psi(t) = re^{-rt}$ describes jumps to $S = S_0$ with reset rate r. $\psi(t)$ transforms $P_0(Y,t)$ to $P(Y,t)$ as [12,13,15]

$$P(Y,t) = e^{-rt}P_0(Y,t) + \int_0^t re^{-r\tau}P_0(Y,\tau)d\tau. \tag{4}$$

For (2) one defines $Y = \ln[S/S_0]$ from the normal distribution, $Y \sim \mathcal{N}([\mu - (\sigma^2/2)]t, \sigma^2 t)$. Multiplying (4) by e^{2Y} and integrating, using $\langle S^2(t)\rangle$ of GBM, one gets

$$\langle S^2(t)\rangle = S_0^2\left(\sigma^2 e^{(\sigma^2-r)t} - r\right)/(\sigma^2 - r). \tag{5}$$

At short times ($|(\sigma^2 - r)t| \ll 1$) Eq. (5) grows linearly,

$$\langle S^2(t)\rangle \approx S_0^2(1+\sigma^2 t). \tag{6}$$

At long times and rare resets ($r_{\mathrm{crit}} = \sigma^2 \gg r$), it grows exponentially with a reduced rate $\langle S^2(t)\rangle \approx S_0^2 e^{(\sigma^2-r)t}$. For frequent resets, $\sigma^2 \ll r$, Eq. (5) starts at short times as (6). At long times, in the nonequilibrium stationary state (NESS), it approaches a plateau (index "pl"),

$$\langle S_{\mathrm{pl}}^2\rangle \approx S_0^2 r/(r-\sigma^2). \tag{7}$$

The first moment, obtained from (4) as $\langle S(t)\rangle = S_0(\mu e^{(\mu-r)t} - r)/(\mu - r)$, gives for the variance

$$\langle (S(t) - \langle S(t)\rangle)^2\rangle = S_0^2\sigma^2\left(e^{(\sigma^2-r)t} - 1\right)/(\sigma^2 - r). \tag{8}$$

For rare resetting it grows linearly at short times,

$$\langle (S(t) - \langle S(t)\rangle)^2\rangle \approx S_0^2\sigma^2 t; \tag{9}$$

at long times $|(\sigma^2 - r)t| \gg 1$, it has a slower exp growth, $\langle (S(t) - \langle S(t)\rangle)^2\rangle \approx S_0^2\sigma^2 e^{(\sigma^2-r)t}/(\sigma^2 - r) \approx \langle S^2(t)\rangle$. For frequent resetting, the variance at short times still follows (9),

*ugdeepakv@gmail.com
†a.cherstvy@gmail.com
‡weiwangnuaa@gmail.com
§rmetzler@uni-potsdam.de
‖igor.sokolov@physik.hu-berlin.de

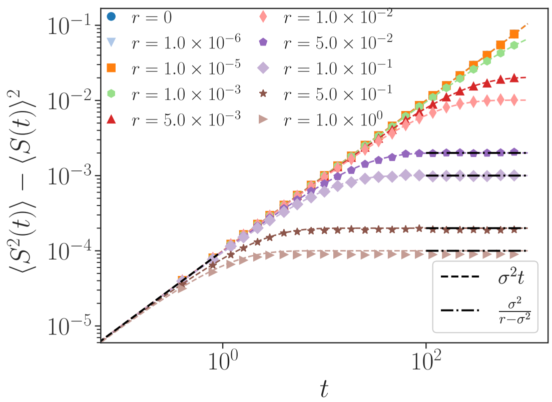

FIG. 1. Variance of reset GBM. Equation (8) is the dotted curves. The legend shows the short- (9) and long-time (10) laws. Reset rates are listed; other parameters are as in Fig. 6.

whereas in the NESS a plateau emerges,

$$\langle (S_{\rm pl} - \langle S_{\rm pl}\rangle)^2\rangle \approx S_0^2\sigma^2/(r-\sigma^2). \tag{10}$$

For the NESS PDF the first term in (4) can be neglected, whereas the integral [after using (2)] becomes

$$P_{\rm pl}(S) \approx \frac{2r\exp[-(2\sigma)^{-1}\sqrt{8r+\sigma^2}|\ln(S/S_0)|]}{\sigma\sqrt{8r+\sigma^2}S(S/S_0)^{1/2}}, \tag{11}$$

that yields (7) for saturating $\langle S_{\rm pl}^2\rangle = \int_0^\infty dS\, P_{\rm pl}(S)S^2$ and (10) for $\langle (S_{\rm pl} - \langle S_{\rm pl}\rangle)^2\rangle = \int_0^\infty dS\, P_{\rm pl}(S)(S-\langle S\rangle)^2$.

In the integrand of $\langle \overline{\delta^2(\Delta)}\rangle$, $\langle [S(t+\Delta)-S(t)]^2\rangle = \langle S^2(t+\Delta)\rangle + \langle S^2(t)\rangle - 2\langle S(t+\Delta)S(t)\rangle$, Eq. (5) is used for $\langle S^2(t)\rangle$ and Ref. [23] yields the correlator. The mean TAMSD of reset GBM at $\mu = 0$, our main result, is

$$\langle \overline{\delta^2(\Delta)}\rangle = \frac{S_0^2\sigma^2}{(\sigma^2-r)}\Bigg[2(e^{-r\Delta}-1) + \frac{(1+e^{(\sigma^2-r)\Delta}-2e^{-r\Delta})(e^{(\sigma^2-r)(T-\Delta)}-1)}{(T-\Delta)(\sigma^2-r)}\Bigg]. \tag{12}$$

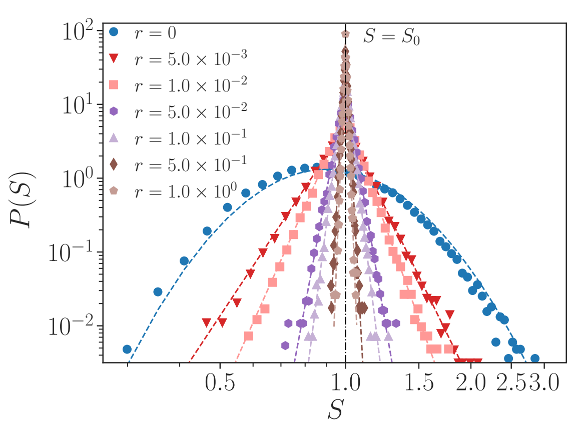

FIG. 2. PDFs of reset GBM. Equation (11) is the dotted colored curves for $P_{\rm pl}(S)$. The PDF $P_0(S)$ (2) is also shown.

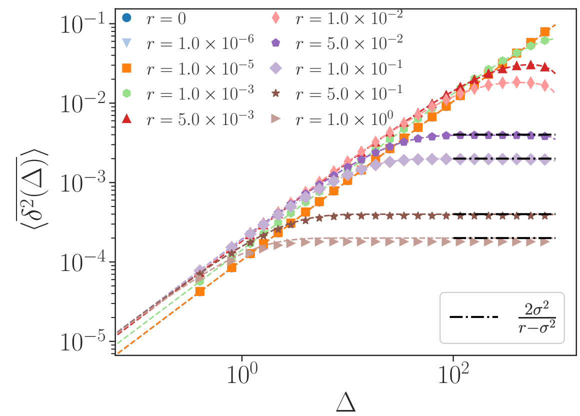

FIG. 3. Mean TAMSDs of reset GBM. Equation (12) is the dotted curves. The NESS asymptote (15) describes the plateaus.

For long trajectories, at $|(\sigma^2 - r)T| \gg 1$, and rare resetting Eq. (12) yields a linear growth at short Δ,

$$\langle \overline{\delta^2(\Delta)}\rangle \approx S_0^2\big(e^{\sigma^2 T}-1\big)\Delta/T, \tag{13}$$

as for GBM (3) [19–21], $\langle \overline{\delta^2(\Delta)}\rangle \approx \langle S^2(T)\rangle\Delta/T$. We, thus, find that generally $\{\langle S^2(\Delta)\rangle, \mathrm{MSD}(\Delta), \mathrm{Var}(\Delta)\} \neq \mathrm{TAMSD}(\Delta)$ at $\Delta/T \ll 1$: ergodicity is weakly broken [22].

For frequent resetting ($r \gg \sigma^2$), long traces ($rT \gg 1$), and short lag times ($\sigma^2\Delta \ll 1$) Eq. (12) starts linearly,

$$\langle \overline{\delta^2(\Delta)}\rangle \approx S_0^2 2\sigma^2 r\Delta/(r-\sigma^2) \approx 2S_0^2\sigma^2\Delta, \tag{14}$$

whereas at long lag times a mean-TAMSD plateau

$$\langle \overline{\delta^2_{\rm pl}}\rangle \approx 2S_0^2\sigma^2/(r-\sigma^2) = 2\langle (S_{\rm pl}-\langle S_{\rm pl}\rangle)^2\rangle \tag{15}$$

emerges. The variance (10)—and not $\langle S_{\rm pl}^2\rangle$ (7) as, e.g., in Ref. [16]—enters in (15) as $S_0 = 1 \neq 0$. For general anomalous-diffusion processes under reset [22] the NESS-conform "equilibration" restores ergodicity [24] in terms of (increment-MSD)(Δ) = TAMSD(Δ) at $\Delta/T \ll 1$.

Reset GBM: Simulations. The Euler-Murayama scheme solves (1) with $S_0 = S(t=0)$ on an interval $[0,T]$ via splitting it into $\bar{N}$ steps [21] with $t_i = t_0 + i\,\Delta t$ and $\Delta t = T/\bar{N} = \delta t$. With $dW(t) \sim \mathcal{N}(0,1)dt$ and $\Delta W_n = W(t_{n+1}) - W(t_n)$, the recurrent prepoint Itô-like [25] algorithm generating a discrete Sisyphus-type [26] reset-GBM walk (Fig. 5) is $S_{n+1} = S_n + \mu S_n\Delta t + \sigma S_n\Delta W_n$ with probability $(1-r\Delta t)$ and $S_{n+1} = S_0$ with $r\,\Delta t$. The results of simulations for the MSD and variance agree excellently with both short- and long-time laws [Eqs. (6), (7) and (9), (10) for Figs. 6 and 1, respectively]. The observed long-time plateaus (10) for frequent resets $r \gg \sigma^2$ are much more sensitive to σ^2/r than (7).

The PDF $P(S,t)$ at long times ($tr \gg 1$) turns into $P_{\rm pl}(S)$, acquires a cusp at $S = S_0$ (*ex post* returns to this price) and shows power-law tails of (11), see Fig. 2 on the log-log scale and Refs. [11,23]. At $r \to 0$, $P(S,t)$ approaches $P_0(S)$ of (2). The precise form of $P_{\rm pl}(S,t)$ follows from comparison of data with an "inverted" (11),

$$\frac{S}{S_0} = \exp\left[\pm\frac{-2\sigma\ln[(2r)^{-1}\sigma\sqrt{8r+\sigma^2}S(S/S_0)^{1/2}P_{\rm pl}(S)]}{\sqrt{8r+\sigma^2}}\right], \tag{16}$$

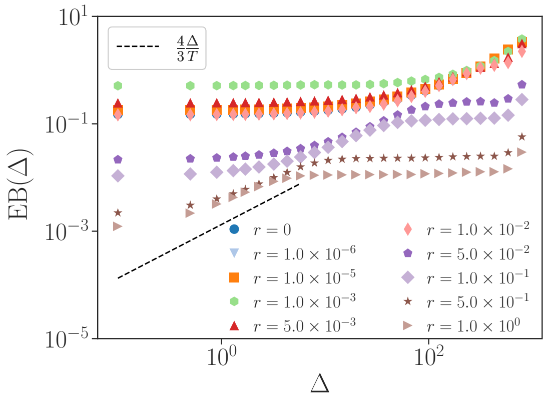

FIG. 4. EB of reset GBM, with the Brownian asymptote [22] $\mathrm{EB}_{\mathrm{BM}}(\Delta) = 4\Delta/(3T)$ shown as the dashed line.

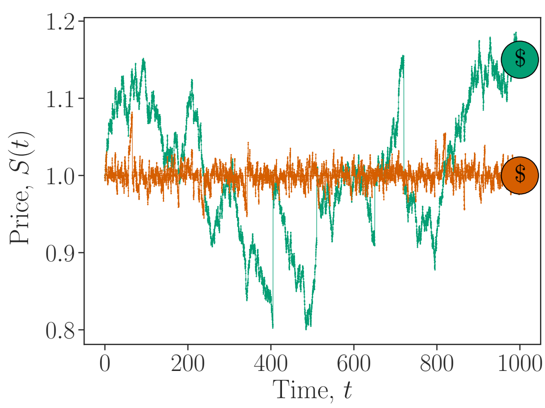

FIG. 5. Trajectories of reset GBM for rare ($r = 0.005$) and frequent ($r = 0.5$) resetting for $\sigma = 10^{-2}$ and $S_0 = 1$.

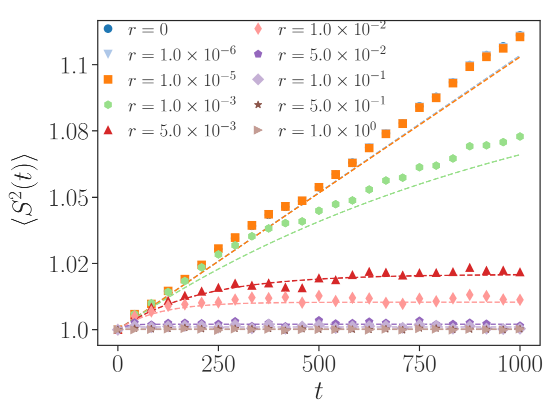

FIG. 6. Simulation results for the MSD of reset GBM with Eq. (5) shown as the dotted curves. Parameters are $S_0 = 1, \sigma = 10^{-2}$, $\mu = 0$, $\delta t = 10^{-1}$, $T = 10^3$, $N = 1.5 \times 10^4$. The same are used in all other plots with simulation results.

versus S/S_0 ["+" ("−") sign reflects $S > S_0$ ($S < S_0$)]. The $P_{\mathrm{pl}}(S)$ data are indeed at the diagonal of Fig. 7; longer NESS-diffusion improves their match with (16).

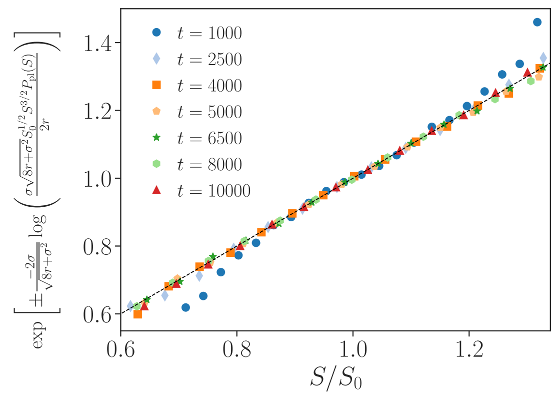

FIG. 7. Inverted PDF in the NESS (16), shown at long times (see the legend for diffusion times), at $r = 10^{-2}$. Quantile-quantile data-versus-theory plots can also be used to validate (11).

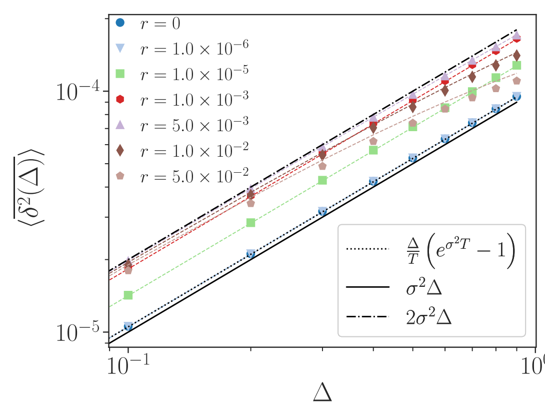

FIG. 8. Short-lag-time TAMSD behavior, zoomed-in from Fig. 3, with the asymptotes for frequent (14) and rare (13) resetting shown (see the legend for r values). The data points for very rare resetting overlap in Figs. 1, 3, 4, 6, 8.

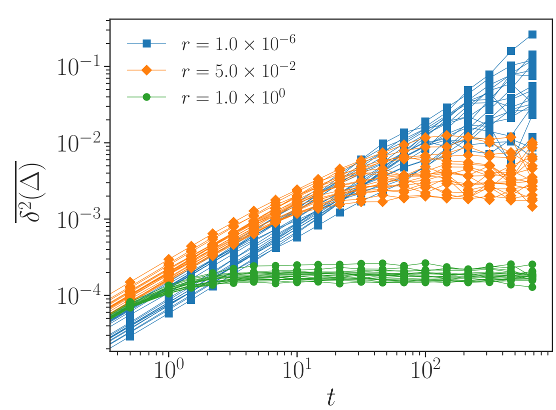

FIG. 9. Distribution of $N = 20$ TAMSD trajectories of reset GBM for several r values and the parameters of Fig. 3.

The evolution of $\langle\overline{\delta^2(\Delta)}\rangle$ fully agrees with (12), Figs. 3 and 8, with short-time laws for rare (13) and frequent (14) resetting—confining $\langle\overline{\delta^2(\Delta \ll r)}\rangle$ between $S_0^2\sigma^2\Delta$ and $2S_0^2\sigma^2\Delta$ (Fig. 8)—and the long-time plateau (15). As GBM

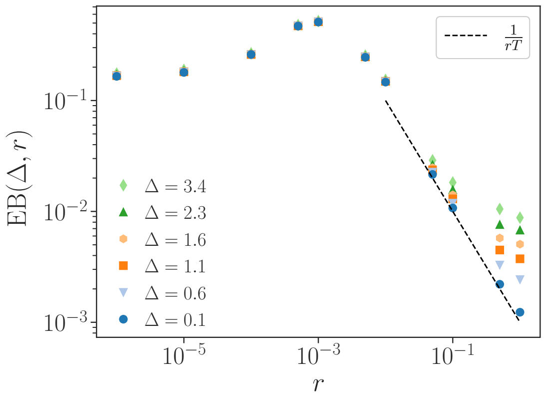

FIG. 10. Short-lag-time EB levels from Fig. 4, following $\mathrm{EB}(\Delta = \delta t) \approx 1/(rT)$ law at frequent resets (alike EB of reset Brownian motion [16]), shown as the dashed line. Nonmonotonicity of $\mathrm{EB}(\delta t, r)$ versus r is also found for other (nonmultiplicative) reset random walks [16]. The long-time frequent-reset EB plateaus in Fig. 4 also follow $\mathrm{EB}_{\mathrm{pl}} \propto 1/r$.

is reset more often, the spread of $\overline{\delta_i^2(\Delta)}$ reduces, Fig. 9, making reset GBM more reproducible and ergodic [smaller EB parameter [22], $\mathrm{EB}(\Delta) = \langle(\overline{\delta^2(\Delta)})^2\rangle/\langle\overline{\delta^2(\Delta)}\rangle^2 - 1$]. EB leveling at $\Delta \to 0$ in Fig. 4 proves pure and reset GBM nonergodic, often with $\mathrm{EB}_{\mathrm{BM}}(\delta t) \ll \mathrm{EB}(\delta t) \approx 1/(rT)$ at $r \gg \sigma^2$, Fig. 10. Overall $\mathrm{EB}(\Delta)$ shape and long-time plateaus $\mathrm{EB}_{\mathrm{pl}}$ are as for other reset [16] and potential-confined [27] walks.

Discussion. Recent debates on nonergodicity in economics [28–30] are extended here to reset GBM. The obtained TAMSD enables to infer σ^2 and r from the time series of reset options [23]. The mean-TAMSD derivation for GBM [19–21] with other reset protocols and, e.g., barrier-crossing resets is feasible [23]. Reference [23] unveils MSD, TAMSD, PDF, and EB behaviors of reset GBM for $\mu > 0$ and all special cases. Model extensions with multiple or distributed and time-varying reset levels $\{S_{0,i}(t)\}$ are possible [23].

Another approach to reset-GBM nonergodicity [18] uses, as compared to process-invariant criterion of MSD-TAMSD equivalence [22] and decay of $\mathrm{EB}(\Delta/T)$ [22,27,31], a nonunique log growth rate "removing" exp growth of GBM [18,28,30], $g(t, N) = \frac{\delta}{\delta t}\ln[\frac{1}{N}\sum_{i=1}^{N} S_i(t)]$. Noncommutativity of $\langle g(t)\rangle = \lim_{N\to\infty} g(t, N)$ and $\widetilde{g(N)} = \lim_{t\to\infty} g(t, N)$ was attributed to nonergodicity of pure [28] and reset [18] GBM [$\langle\overline{\delta^2(\Delta)}\rangle$ [19–21] was not computed]. Mean $g(t, N)$ and "median" $g'(t, N) = \frac{\delta}{\delta t}\{\frac{1}{N}\sum_{i=1}^{N}\ln[S_i(t)]\}$ rates differ also in GBM-based models of wealth growth [30].

Acknowledgments. A.G.C. thanks HU Berlin and R.M. thanks FNP and DFG (Grant No. ME 1535/12-1) for support.

[1] M. B. Goldman, H. B. Sosin, and M. A. Gatto, J. Fin. **34**, 1111 (1979).
[2] A. Conze and S. Viswanathan, J. Fin. **46**, 1893 (1991).
[3] M. Rubinstein and E. Reiner, Risk **4**, 28 (1991).
[4] S. F. Gray and R. E. Whaley, J. Derivatives **5**, 99 (1997).
[5] H. He, W. P. Keirstead, and J. Rebholz, Math. Fin. **8**, 201 (1998).
[6] S. F. Gray and R. E. Whaley, Aust. J. Man. **24**, 1 (1999).
[7] P. P. Boyle and Y. Tian, J. Fin. Quant. An. **34**, 241 (1999).
[8] W.-Y. Cheng and S. Zhang, J. Derivatives **8**, 59 (2000).
[9] D. Davydov and V. Linetsky, Manag. Sci. **47**, 949 (2001).
[10] V. Linetsky, Fin. Stochast. **8**, 373 (2004).
[11] S. C. Manrubia and D. H. Zanette, Phys. Rev. E **59**, 4945 (1999).
[12] M. R. Evans and S. N. Majumdar, Phys. Rev. Lett. **106**, 160601 (2011).
[13] S. N. Majumdar and G. Oshanin, J. Phys. A: Math. Theor. **51**, 435001 (2018).
[14] A. S. Bodrova, A. V. Chechkin, and I. M. Sokolov, Phys. Rev. E **100**, 012119 (2019).
[15] M. R. Evans, S. N. Majumdar, and G. Schehr, J. Phys. A: Math. Theor. **53**, 193001 (2020).
[16] W. Wang, A. G. Cherstvy, H. Kantz, R. Metzler, and I. M. Sokolov, Phys. Rev. E **104**, 024105 (2021).
[17] D. H. Zanette and S. Manrubia, Chaos **30**, 033104 (2020).
[18] V. Stojkoski, T. Sandev, L. Kocarev, and A. Pal, Phys. Rev. E **104**, 014121 (2021).
[19] A. G. Cherstvy, D. Vinod, E. Aghion, A. V. Chechkin, and R. Metzler, New J. Phys. **19**, 063045 (2017).
[20] S. Ritschel, A. G. Cherstvy, and R. Metzler, J. Phys.: Compl. **2**, 045003 (2021).
[21] A. G. Cherstvy, D. Vinod, E. Aghion, I. M. Sokolov, and R. Metzler, Phys. Rev. E **103**, 062127 (2021).
[22] R. Metzler, J.-H. Jeon, A. G. Cherstvy, and E. Barkai, Phys. Chem. Chem. Phys. **16**, 24128 (2014).
[23] D. Vinod, A. G. Cherstvy, R. Metzler, and I. M. Sokolov (unpublished).
[24] W. Wang, A. G. Cherstvy, R. Metzler, and I. M. Sokolov (unpublished).
[25] I. M. Sokolov, Chem. Phys. **375**, 359 (2010).
[26] M. Montero and J. Villarroel, Phys. Rev. E **94**, 032132 (2016).
[27] A. G. Cherstvy, S. Thapa, Y. Mardoukhi, A. V. Chechkin, and R. Metzler, Phys. Rev. E **98**, 022134 (2018).
[28] O. Peters and W. Klein, Phys. Rev. Lett. **110**, 100603 (2013).
[29] O. Peters, Nat. Phys. **15**, 1216 (2019).
[30] A. Adamou and O. Peters, Significance **13**, 32 (2016).
[31] A. G. Cherstvy, H. Safdari, and R. Metzler, J. Phys. D: Appl. Phys. **54**, 195401 (2021).